Bull. Mater. Sci., Vol. 25, No. 3, June 2002, pp. 175–180. © Indian Academy of Sciences.

# Synthesis and characterization of sol–gel derived ZnS : $Mn^{2+}$ nanocrystallites embedded in a silica matrix

**B BHATTACHARJEE, D GANGULI, K IAKOUBOVSKII†, A STESMANS† and S CHAUDHURI***

Department of Materials Science, Indian Association for the Cultivation of Science, Kolkata 700 032, India
†Department of Physics, Katholieke Universiteit Leuven, 3001 Leuven, Belgium

MS received 22 April 2002

**Abstract. Synthesis and characterization of undoped and $Mn^{2+}$ doped ZnS nanocrystallites (radius 2–3 nm) embedded in a partially densified silica gel matrix are presented. Optical transmittance, photoluminescence (PL), ellipsometric and electron spin resonance measurements revealed manifestation of quantum size effect. PL spectra recorded at room temperature revealed broad blue emission signal centred at ~ 420 nm and $Mn^{2+}$ related yellow–orange band centred at ~ 590 nm while ESR indicated that Mn in ZnS was present as dispersed impurity rather than Mn cluster.**

**Keywords. Zinc sulphide; sol–gel; nanoparticles; luminescence; ESR.**

## 1. Introduction

Zinc sulphide with low Mn doping level is an efficient phosphor (Toyama *et al* 2000), used in the form of powder and thin films. In nanoparticle form, ZnS : $Mn^{2+}$ exhibits additional interesting electro-optical and other properties (Zeinert *et al* 1994). There are various techniques for the preparation of ZnS : $Mn^{2+}$ nanoparticles, the two most popular ones being synthesis in colloidal solutions or in reverse micelles (Jin *et al* 1996; Smith and Zhang 2000). The nanoparticles thus generated require capping by e.g. suitable thiols in order to avoid quick degradation or agglomeration. Another route may be synthesis in 'controlled pore' solid materials like zeolites or rigid gels. Gels are interesting because their precursors, i.e. sols, can easily be amenable to the formation of thin films. Confinement of the nanoparticles within the pores of rigid solid materials also hinders their degradation or agglomeration. Thin solid films with dispersed luminescent nanoparticles (as against colloidal dispersions) also have the advantage that they can be used readily as parts of optical (e.g. luminescent) devices.

In spite of the advantage of the sol–gel method in facile preparation of luminescent ZnS : $Mn^{2+}$ nanoparticles dispersed in a thin solid dielectric film, only limited work has been done in this area (Saenger *et al* 1998; Sohling *et al* 1998). In the present work, $Mn^{2+}$ doped ZnS nanoparticles have been synthesized by the sol–gel method in an amorphous silica thin film matrix. The composite films thus obtained were studied for their optical absorption, luminescence and electron spin resonance (ESR) properties in an attempt to characterize the possible $Mn^{2+}$ sites in the ZnS structure.

## 2. Experimental

### 2.1 *Preparation of sols and films*

The sol required for deposition of the films was prepared in two parts. In the first part, tetraethyl orthosilicate, $Si(OC_2H_5)_4$ (TEOS, for synthesis, Merck. Schuchard) was dissolved in a solution of 2-propanol (pro analysi, Merck., India, dried over molecular sieve activated under agitation) and distilled water. Hydrochloric acid (0·1 N, Titrisol, Merck., India) was added in this solution as a catalyst and it was stirred for ~ 1 h.

To prepare another part of the sol, $Zn(NO_3)_2 \cdot 6H_2O$ (Purified, Merck., India) was dissolved in a solution of 2-propanol and distilled water to obtain the zinc precursor. Thiourea, $NH_2CSNH_2$ (Pure, Merck., India) was dissolved in this solution as the source of sulphur. Five at.% $Zn^{2+}$ was substituted by $Mn^{2+}$ in the solution through Mn $(CH_3COO)_2 \cdot 2H_2O$ (Pure, Merck., India) and this solution was stirred for ~ 2 h.

The two parts of the sol were mixed under stirring to obtain a clear and transparent sol. This final sol was then again stirred for 2 h before the films were prepared. In this sol, the equivalent molar ratio of $SiO_2$ : (metal sulphide) was fixed at 70 : 30. For comparison, sols were also prepared for synthesis of undoped ZnS films.

The final sol was used to prepare films by spin coating (~ 3000 rpm) on quartz glass substrates (25 × 25 $mm^2$)

*Author for correspondence

for optical and ESR studies and on carbon coated Cu grid for microstructural (TEM) study. The films were then (in less than ~ 10 s) transferred to an oven preset at the required annealing temperature (flash heating at 573 K for 30 min).

### 2.2 *Characterization of the films*

Optical studies were performed by measuring transmittance in the wavelength region $l$ = 200–800 nm using a spectrophotometer (Hitachi-U3410) at room temperature. The spectra were recorded with a resolution of $l$ ~ 0·07 nm along with a photometric accuracy of ± 0·3% for transmittance measurements. Microstructure of the films was studied with TEM (Hitachi H-600). ESR measurements were performed at 300 K in a commercial Bruker Q band spectrometer (~ 34 GHz), under conditions of slow adiabatic passage. The $g$ values and absolute intensities of ESR signals were determined using a thoroughly calibrated LiF : Li standard (Stesmans and Van Gorp

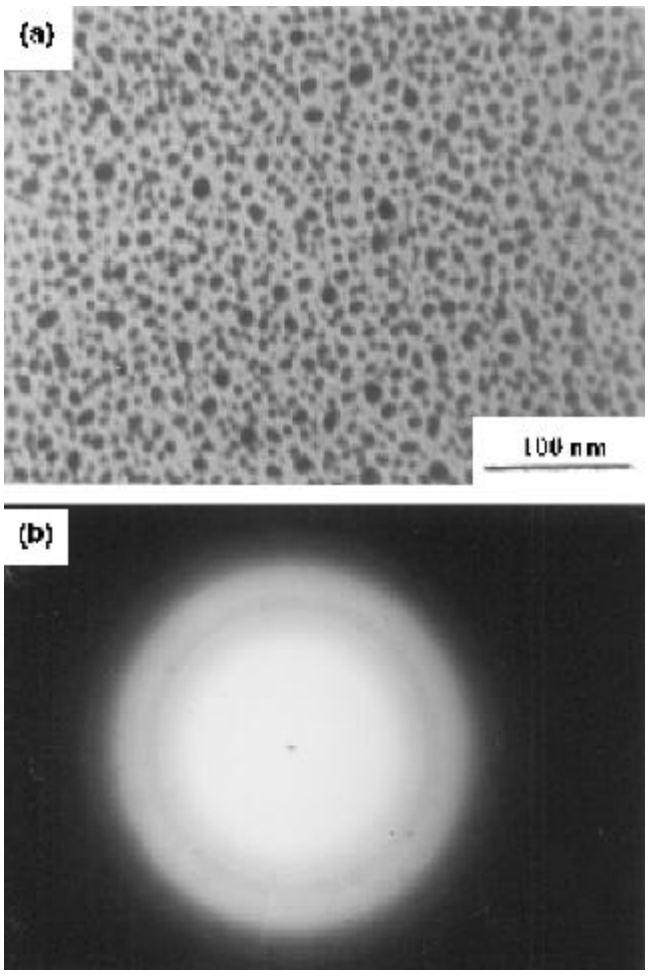


**Figure 1.** Transmission electron micrograph (**a**) and electron diffraction pattern (**b**) of a representative nanocrystalline $Mn^{2+}$ doped (5 at.%) ZnS film.

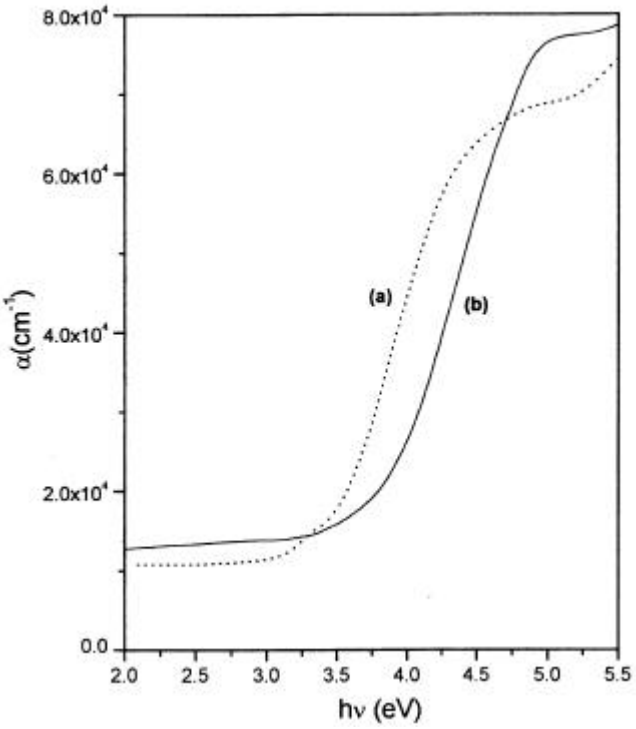


**Figure 2.** Variation of optical absorption coefficient ($a$) with photon energy ($hn$) (**a**) for undoped and (**b**) $Mn^{2+}$ doped (5 at.%) nanocrystalline ZnS film.

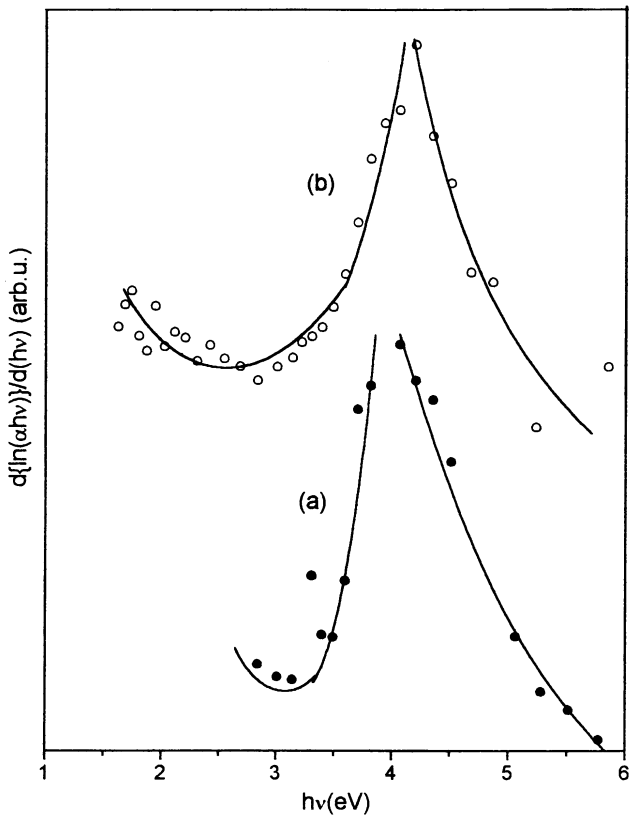


**Figure 3.** $d\{\ln(ahn)\}/d(hn)$ vs $hn$ plots for (**a**) undoped and (**b**) $Mn^{2+}$ doped nanocrystalline ZnS film ($a$ in $cm^{-1}$, $hn$ in eV).

1989a,b) co-mounted with the sample. Photoluminescence (PL) spectra were recorded at 300 K using a Perkin Elmer LS55 spectrometer with excitation wavelengths of 250 nm and 400 nm to detect the blue and yellow–orange emissions, respectively. Ellipsometric data for the films were recorded in a Spectroscopic Phase Modulated Ellipsometer (UVISEL$^{TM}$ 460, ISA JOBIN-YVON SPEX) in the range $l$ = 300–1200 nm.

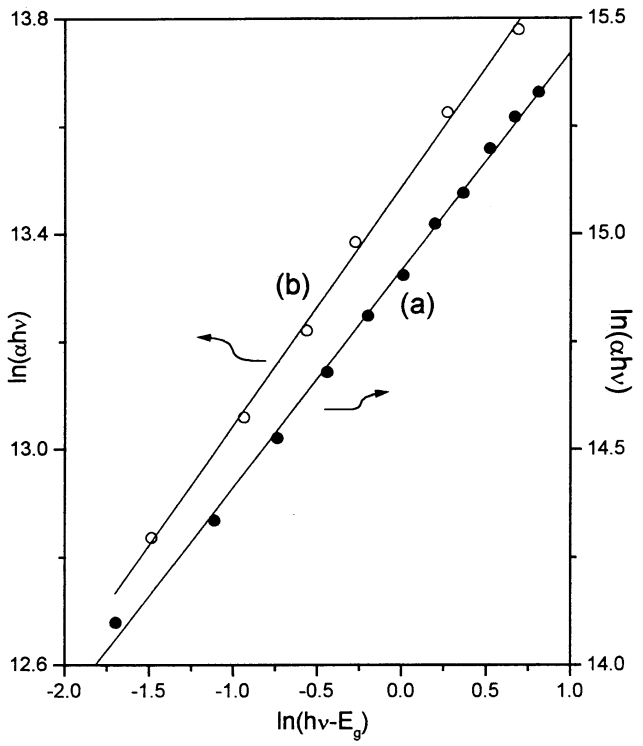


**Figure 4.** ln($ahn$) vs ln($E_g - hn$) plots for (**a**) undoped and (**b**) $Mn^{2+}$ doped nanocrystalline ZnS film ($a$ in $cm^{-1}$, $hn$ in eV and $E_g$ in eV).

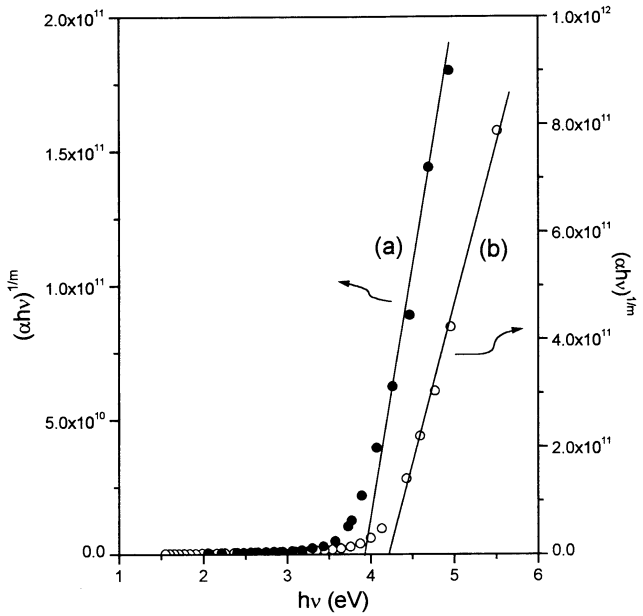


**Figure 5.** Plot of $(ahn)^{1/m}$ vs $hn$ for (**a**) undoped and (**b**) $Mn^{2+}$ doped nanocrystalline ZnS film ($a$ in $cm^{-1}$, $hn$ in eV).

## 3. Results and discussion

### 3.1 *Microstructural studies*

Micrograph (TEM) of a representative ZnS : Mn film (5 at.% doped) and the corresponding diffraction pattern are shown in figures 1a and b, respectively. Presence of fine ZnS nanoparticles in silica matrix is clearly visible in the TEM picture (figure 1a), while the corresponding diffraction pattern of the film consists of a central halo with concentric broad rings, the broadness possibly originating from the confinement of the nanocrystallites embedded in the silica matrix. The rings correspond to reflections from the (111) and (200) planes, thus confirming the cubic crystallographic structure of the ZnS nanoparticles. The average radii ($r$) of the nanocrystallites determined from TEM are 2·5 nm (± 0·5 nm) and 3 nm (± 0·5 nm) for doped and undoped films, respectively. The ratio of particle diameters to the interparticle separations ($h = d/s$), which is a measure of dispersibility of the particles in a dielectric matrix, has an average value of ~ 0·8 and ~ 0·75 for doped and undoped films, respectively. This moderately high value of $h$ (close to unity) suggests that the particles were neither agglomerated nor situated at large distances apart from each

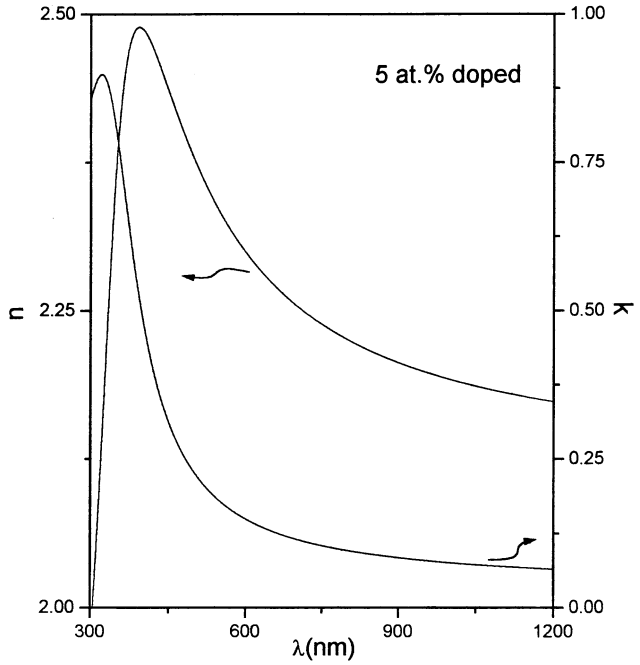


**Figure 6.** Variations of refractive index ($n$) and extinction coefficient ($k$) with wavelength ($l$) for 5 at.% $Mn^{2+}$ doped nanocrystalline ZnS film.

other, but well dispersed in the silica matrix, which prevented the particles from fast degradation or agglomeration in spite of the relatively high loading of sulphide nanoparticles in the silica matrix (Minti *et al* 1991; Guglielmi *et al* 1997).

### 3.2 *Optical absorption and optical bandgap*

The absorption coefficient ($a$) was determined from the transmittance vs wavelength ($l$) traces recorded in the region $l$ = 200–800 nm for undoped (figure 2a) and doped (figure 2b) films. The absorption coefficient ($a$) may be written as (Bhattacharyya *et al* 1992)

$$a = A(hn - E_{gi})^m/hn, \quad (1)$$

where $E_{gi}$ is the band gap corresponding to a particular transition occurring in the film and $m$ characterizes the nature of transition. The value of $m$ may be 1/2, 2, 3/2 and 3 corresponding to the allowed direct, allowed indirect, forbidden direct and forbidden indirect transitions, respectively (Pankove 1971). When allowed direct transition is pre-assumed, as usually done by the workers, band gap may be obtained from extrapolation of the straight line portion of the $(ahn)^2$ vs $hn$ plot to $a = 0$. But, in the nanocrystalline film there may be deviation from bulk like transition. So, $m$ value should be determined without any pre-assumption of the nature of transition. Now, from (1) we obtain

$$d\{\ln (ahn)\}/d(hn) = m_i/(hn - E_{gi}), \quad (2)$$

which suggests that a plot of $d\{\ln(ahn)\}/d(hn)$ vs $hn$ (derivative spectra) will indicate a divergence at an energy value, $E_g$, where a transition takes place. Plots of the derivative spectra for undoped and doped films are shown in figures 3a and b, respectively. The discontinuities in the plots were observed at 3·95 and 4·2 eV for the undoped and doped films, respectively. With a view to determining the nature of transition (or $m$ value) ln ($ahn$) vs ln($hn - E_g$) was plotted (figure 4) which was a straight line with slope $m$. Thus, $m$ values of 0·49 and 0·46 were deduced for undoped and doped films, respectively. The $m$ values thus obtained were close to 0·5 (as expected for allowed direct transition in bulk ZnS). The exact values of band gaps corresponding to the $m$ values mentioned above were obtained from the $(ahn)^{1/m}$ vs $hn$ plots (figure 5).

It may be noticed that the band gap values are higher than the bulk value for ZnS (3·6 eV) due to quantum confinement in the ZnS nanocrystallites. It may be

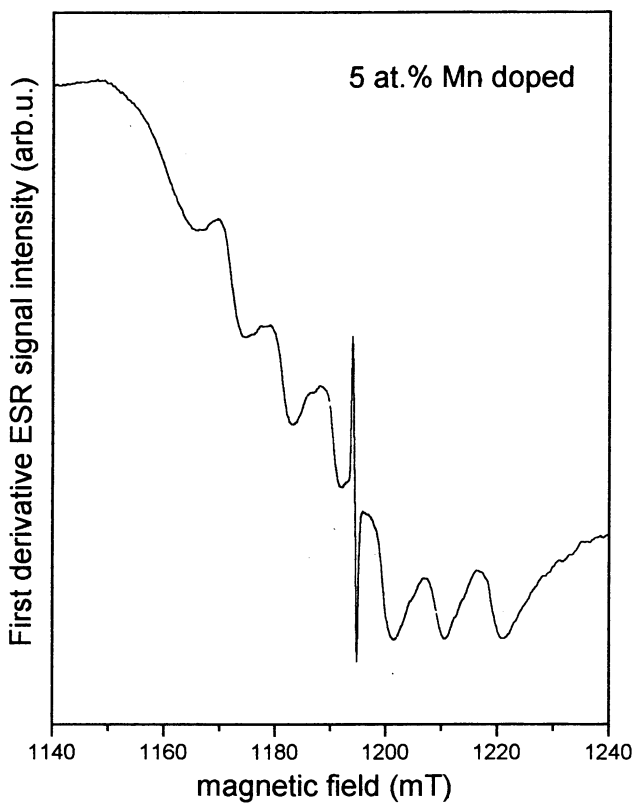


**Figure 7.** Variation of the first derivative of ESR signal intensity with magnetic field for $Mn^{2+}$ doped (5 at.%) nanocrystalline ZnS film.

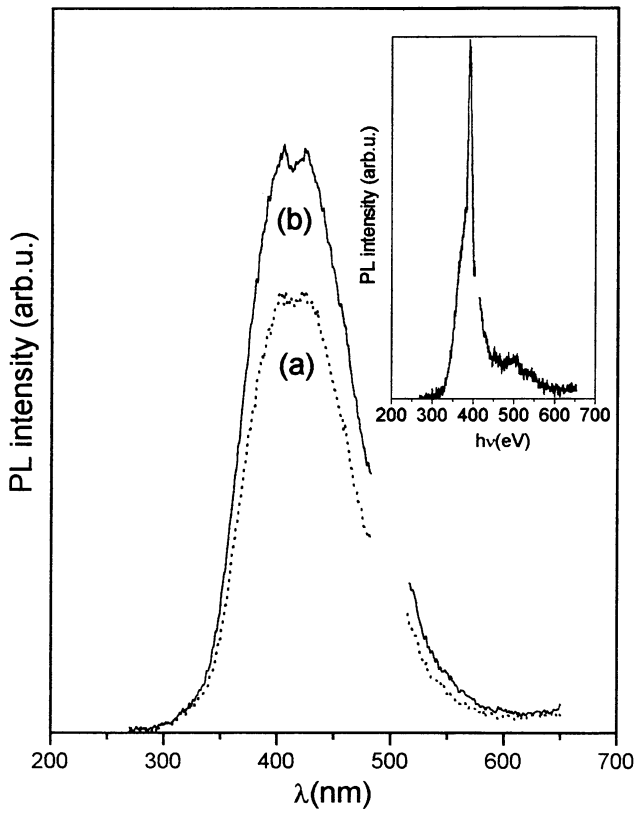


**Figure 8.** PL spectra for (**a**) undoped and (**b**) $Mn^{2+}$ doped nanocrystalline ZnS film recorded at 300 K under 250 nm excitation. Inset shows PL emission from bare substrate under 200 nm excitation.

noticed that the band gap in the Mn doped ZnS film was higher than that of undoped film because the grain size in the doped film was lower (~ 2·5 nm) than that in undoped film (~ 3 nm) depending on the preparative conditions of the films.

The properties of nanocrystalline materials show deviation from the corresponding bulk properties when the sizes of the crystallites become comparable to the Bohr excitonic radius ($a_B$) given by

$$a_B = 4pe\,\hbar^2[1/m^*_e + 1/m^*_h]/e^2, \quad (3)$$

where $e$ is the dielectric constant, and $m^*_e$ and $m^*_h$ are the effective masses of electrons and holes, respectively. From (3) the excitonic Bohr radius of ZnS can be determined as 2·5 nm using the values of $e = 8{\cdot}76$, $m^*_e = 0{\cdot}34\ m_0$ and $m^*_h = 0{\cdot}23\ m_0$ (Landolt-Bornstein 1987). The values of grain sizes in the nanocrystalline ZnS films, as determined from TEM studies, are comparable to $a_B$ supporting the quantum-size effect. Further, the blue shift of the band gap ($\Delta E_g$) could also be utilized to determine the crystallite radius ($r$) using the relation (Brus 1984; Yuang *et al* 1994)

$$\Delta E_g = E_{g(film)} - E_{g(bulk)} = [\hbar^2 p^2/2\ \mu r^2] - [1{\cdot}8\ e^2/e\ r], \quad (4)$$

where $\mu$ is the reduced electron–hole effective mass.

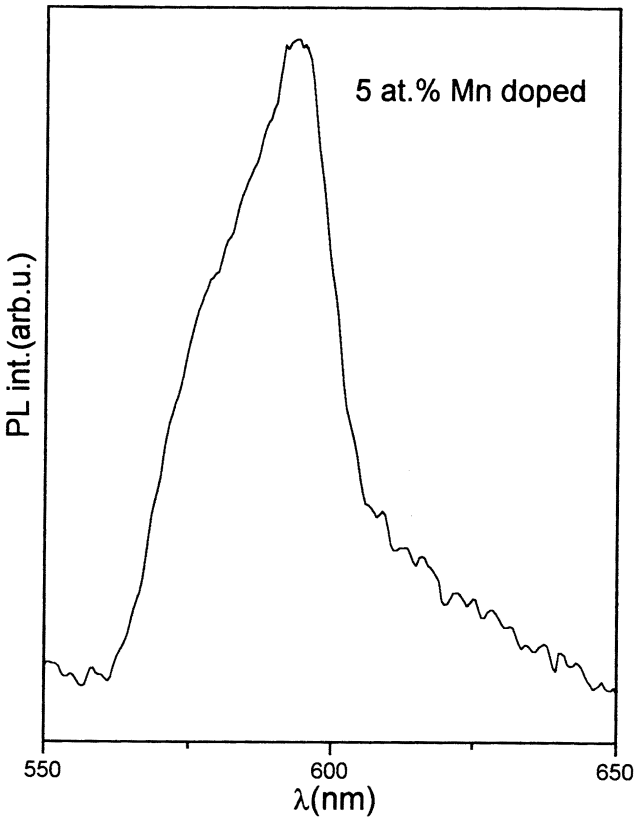


**Figure 9.** Photoluminescence spectra for 5 at.% $Mn^{2+}$ doped nanocrystalline ZnS film recorded at 300 K under 400 nm excitation.

Using (4), the particle sizes were determined as $r$ = 2·8 nm and 2·12 nm in case of undoped and doped ZnS nanocrystalline films, respectively. These $r$ values were comparable to those obtained from TEM studies.

### 3.3 *Ellipsometric study*

The film thickness ($t$) and refractive index ($n$) were obtained from the ellipsometric analysis. The film thicknesses were in the range 120–135 nm for both undoped and doped films. At 550 nm, doped ZnS film exhibited $n$ ~ 2·33 whereas it was 2·36 for undoped ZnS film. The dispersion curves of refractive index ($n$) and extinction coefficient ($k$) for the doped film are shown in figure 6. The high-frequency dielectric constant ($e$) was determined from these $n$ and $k$ data in the region of the film transparency (> 500 nm). The value of $e$ thus obtained (~ 5·47 at 550 nm) was lower than that of the bulk ZnS ($n$ = 2·35) (Nicolau and Menard 1988). This reduction in $e$ may be attributed to the quantum confinement effect in nanocrystalline film which led to the reduction of $n$ with decreasing particle size as was discussed by Yoffe (2001).

### 3.4 *ESR study*

ESR measurements were reported by different workers (Kennedy *et al* 1995; Yeom *et al* 1996; Igarashi *et al* 2001) to study the symmetry, electronic structure and coordination state of Mn impurity in ZnS : Mn powders and thin films. Several Mn-related signals might be expected from the results of previous studies of ZnS composites (Igarashi *et al* 1997). However, in the present work only one has been detected. Figure 6 shows the ESR spectra for a Mn doped film (containing 5 at.% Mn) recorded using microwave power of 10 mW and a modulation amplitude of 0·5 mT. The central sharp line was due to a LiF ESR marker {$g$ = 2·002293 (Stesmans and Van Gorp 1989a,b)}. A sextet of relatively broad lines, observed in figure 7, was fitted with isotropic $g$ factor of

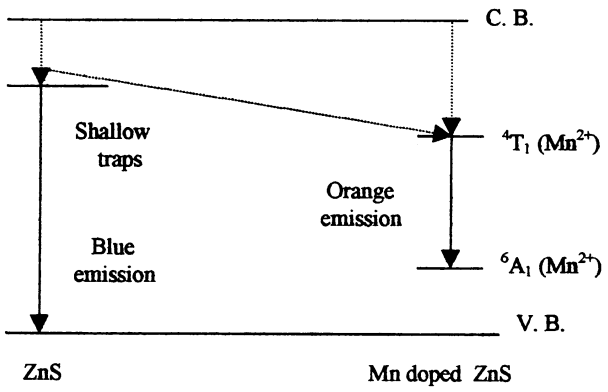


**Figure 10.** A schematic band diagram for $Mn^{2+}$ doped ZnS.

2·0008 and hyperfine constant $|A| = 88{\cdot}9$ mT. Similar parameters were deduced by Kennedy *et al* (1995) for nano ZnS ($g = 2{\cdot}001$ and $|A| = 89$ mT). The observed characteristic sextet structure of ESR spectra suggested that Mn in ZnS was present as dispersed $Mn^{2+}$ impurities rather than Mn clusters. Yeom *et al* (1996) observed that Mn formed clusters for doping > 1 at.% in their ZnS : Mn powder and thin films as indicated by the broad resonance band in the ESR signals despite the hyperfine sextet. In the present case, up to 5 at.% Mn could be incorporated without clustering possibly due to the presence of nanocrystallites embedded in the $SiO_2$ matrix producing an effective capping. Thus, $SiO_2$ played an important role to make the nanoparticles well dispersed. Unfortunately, the Mn sites, corresponding to the detected ESR signals, have not been reliably identified yet.

### 3.5 *Photoluminescence study*

Room-temperature photoluminescence (PL) spectra of the samples (on quartz substrate) along with PL from bare substrate are presented in figures 8 and 9. When the films were excited at 200 nm, strong luminescence at 390 nm appeared from bare quartz glass substrate (inset, figure 8). This luminescence did not occur when the films were excited with 250 nm. All the samples were excited at 250 nm to detect the emission signal (eliminating substrate effect). The break in the spectra at ~ 500 nm was due to subtraction of the second order of the excitation peak.

When the samples were excited at 250 nm, broad blue emission was observed at ~ 420 nm. Slight red shift in this blue band with increasing particle size was noticed for the undoped films. On the other hand, when the samples were excited at ~ 400 nm and the emission spectra were recorded in the region 550–650 nm, yellow–orange emission centred at ~ 590 nm was observed. In the present case, the luminescence was the characteristic for the $^4T_1 \rightarrow {}^6A_1$ transition in $Mn^{2+}$ ions (figure 10) in a ZnS matrix (Sooklal *et al* 1996; Suyver *et al* 2001).

## 4. Conclusions

The films of undoped and $Mn^{2+}$ doped (5 at.%) ZnS nanoparticles embedded in $SiO_2$ matrix consisted of well dispersed nearly monosized nanoparticles with the value of the index of dispersibility ~ 0·8. Microstructural, optical and ellipsometric studies revealed that quantum size effect occurred in the films. ESR study indicated dispersed $Mn^{2+}$ impurity rather than Mn cluster in the Mn doped ZnS films. Mn could be incorporated up to 5 at.% without clustering possibly due to the presence of nanocrystallites embedded in the $SiO_2$ matrix producing an effective capping. The films exhibited surface state related blue emission (excited at ~ 250 nm) of ZnS nanoparticle in addition to characteristic yellow–orange emission (excited at ~ 400 nm) centred at ~ 590 nm for Mn doped films due to the $^4T_1 \rightarrow {}^6A_1$ transition in $Mn^{2+}$ ions.

## Acknowledgements

The authors would like to thank Dr D Bhattacharyya and Dr S K Mandal for their help in recording the ellipsometric data and photoluminescence spectra, respectively. Authors are also grateful to Mr N Chaudhuri for recording the transmission electron micrographs and diffraction patterns. One of the authors (SC) would like to express sincere gratitude to DAE-BRNS for their interest in the present work.

## References

Bhattacharyya D, Chaudhuri S and Pal A K 1992 *Vacuum* **43** 313

Brus L E 1984 *J. Chem. Phys.* **80** 4403

Guglielmi M, Martucci A and Menegazzo E 1997 *J. Sol–Gel Sci. Technol*. **8** 1017

Igarashi T, Ihara M, Kusunoki T, Ohno K, Isobe T and Senna M 2001 *J. Nanoparticle Res.* **3** 51

Igarashi T, Isobe T and Senna M 1997 *Phys. Rev*. **B56** 6444

Jin C, Yu J, Sun L, Dou K, Hou S, Zhao J, Chen Y and Huang S 1996 *J. Lumin*. **66 & 67** 315

Kennedy T A, Glaser E R and Klein P B 1995 *Phys. Rev*. **B52** 356

Landolt-Bornstein 1987 *Numerical data and functional relationships in science and technology* (Berlin: Springer Verlag) **Vol. 22a,** p. 168

Minti H, Eyal M and Reisfeld R 1991 *Chem. Phys. Lett*. **183** 277

Nicolau Y F and Menard J C 1988 *J. Cryst. Growth* **92** 128

Pankove J I 1971 *Optical processes in semiconductors* (New Jersey, USA: Prentice Hall) p. 34

Saenger D U, Jung G and Mennig M 1998 *J. Sol–Gel Sci. Technol.* **13** 635

Smith B A, Zhang J Z, Joly A and Liu J 2000 *Phys. Rev.* **B62** 2021

Sohling U, Jung G, Saenger D U, Lu S, Kutsch B and Mennig M 1998 *J. Sol–Gel Sci. Technol*. **13** 685

Sooklal K, Cullum B S, Angel S M and Murphy C J 1996 *J. Phys. Chem*. **100** 4551

Stesmans A and Van Gorp G 1989a *Rev. Sci. Instrum*. **60** 2949

Stesmans A and Van Gorp G 1989b *Phys. Lett.* **A139** 95

Suyver J G, Wuister S F, Kelly J J and Meijerink A 2001 *Nano Lett*. **1** 429

Toyama T, Adachi D and Okamoto H 2000 *Mater. Res. Soc. Symp. Proc*. **621** Q4.4.1

Yeom T H, Lee Y H, Hahn T S and Oh M H 1996 *J. Appl. Phys*. **79** 1004

Yoffe A D 2001 *Adv. Phys*. **50** 1

Yuang Y S, Chen Y F, Lee Y Y and Liu L C 1994 *Jpn J. Appl. Phys.* **76** 3041

Zeinert A, Benalloul P, Benoit J, Barthou C and Gumlich H E 1994 *J. Cryst. Growth* **138** 1023